Structure of molten yttrium aluminates: a neutron diffraction study

2007 J. Phys.: Condens. Matter 19 415105

(http://iopscience.iop.org/0953-8984/19/41/415105)

IOP PUBLISHING JOURNAL OF PHYSICS: CONDENSED MATTER

J. Phys.: Condens. Matter **19** (2007) 415105 (11pp) doi:10.1088/0953-8984/19/41/415105

Structure of molten yttrium aluminates: a neutron diffraction study

V Cristiglio[1,2], L Hennet[1], G J Cuello[2], I Pozdnyakova[1], M R Johnson[2], H E Fischer[2], D Zanghi[1], Q Vu Van[3], M C Wilding[3], G N Greaves[3] and D L Price[1]

[1] Centre de Recherche sur les Matériaux à Haute Température, CNRS-CRMHT, 1d avenue de la Recherche Scientifique, 45071 Orléans cedex 2, France
[2] Institut Laue-Langevin, 6 rue Jules Horowitz, BP48 Grenoble cedex 9, France
[3] Institute of Mathematical and Physical Sciences, University of Wales, Aberystwyth SY23 3BZ, UK

E-mail: cristiglio@ill.fr

Received 30 April 2007, in final form 29 July 2007
Published 27 September 2007
Online at stacks.iop.org/JPhysCM/19/415105

Abstract

We used the aerodynamic levitation technique combined with CO_2 laser heating to study the structure of liquid yttrium aluminates above their melting point with neutron diffraction. For various yttria contents, we determined the structure factors and corresponding pair correlation functions describing the short-range order in the liquids. In particular, we derived Al–O and Y–O bond distances and coordination numbers. Experimental data are compared with *ab initio* molecular dynamics, carried out using the VASP code where the interatomic forces are obtained from density functional theory. In particular, partial pair correlation functions have been calculated and are in relatively good agreement with the experimental observations.

1. Introduction

Yttrium aluminates $(Y_2O_3)_x$–$(Al_2O_3)_{1-x}$, where x stands for the yttria content, are interesting materials for various reasons. In particular, some works have reported evidence of the existence of a liquid–liquid phase transition between a high-density amorphous (HDA) form and one with a lower density (LDA form) that should be present during sample supercooling [1–3]. These two forms observed by using scanning electron microscopy on the obtained glasses have the same chemical composition, but their density differs by about 4%. Various x-ray and neutron measurements [4, 5] and molecular dynamics simulations [6] have been made to try to explain this behaviour.

From a technological point of view, mixtures of Y_2O_3 and Al_2O_3 produce several important compounds, particularly the garnet $Y_3Al_5O_{12}$ or YAG ($x = 0.375$), the perovskite $YAlO_3$ (YAP, $x = 0.5$) and the monoclinic phase $Y_4Al_2O_9$ (YAM, $x = 0.667$). When doped with rare earths, YAG single crystals can be used in pumped lasers [7] or for making scintillators [8]. These

crystals are grown from the melt using the Czochralski method and knowledge of the liquid properties is therefore important.

Finally, some studies reported that YAG presents a surprising behaviour during solidification with two different routes [9, 10]. In particular, depending on the temperature reached by the melt, the material can crystallize either as a single garnet phase or as a mixture of YAP and Al_2O_3.

Studies of the liquid structure of these compounds are therefore interesting from both fundamental and technological points of view. Due to their high melting points (above 2090 K) [11] and the risk of contamination with a crucible at these temperatures, only a few structural studies have been performed with methods that can be combined with levitation techniques. These include nuclear magnetic resonance [12], x-ray and neutron scattering [13, 14] and x-ray absorption spectroscopy [15]. All these studies concern the composition of YAG and a very small number of works are related to other compositions, including a recent x-ray study [16]. Up to now, nothing has been done with neutron diffraction.

In this paper, we present new results on the structure of levitated liquid yttrium aluminates obtained with neutron diffraction. In particular, we studied various compositions from $x = 0.150$ up to $x = 0.375$. An experimental description of the short-range order is presented and compared with results from *ab initio* molecular dynamics (AIMD) simulations.

2. Technical details

2.1. Sample preparation

In this work a sol–gel method was used for synthesizing $(Y_2O_3)_x$-$(Al_2O3)_{1-x}$ powders. Three compositions were studied: $x = 0.150$ (AY15), 0.250 (AY25) and $x = 0.375$ (YAG). Spherical samples were prepared by melting the powders, previously pressed under a pressure of 200 MPa, in an aerodynamic levitator with a CO_2 laser beam and then cooled down to room temperature. They had a nominal diameter between 2.7 and 3 mm, corresponding to weights of about 40–60 mg.

2.2. Heating system

For these experiments, we used an aerodynamic levitation setup specially designed for neutron diffraction experiments. Figure 1 is a schematic view of the levitation setup integrated into the D4c diffractometer at the Institut Laue-Langevin (ILL) in Grenoble (France). This device is described in detail in Hennet *et al* [17] and we give here a short description of the working principle.

The spherical sample is levitated in a convergent–divergent nozzle under an argon–oxygen (3%) gas flow and heated to the desired temperatures by two 125 W CO_2 lasers directed from above. The laser beams are focused on the sample by means of spherical mirrors at two different angles in order to obtain a homogeneous temperature distribution. Two NaCl windows are used to transmit the beam into the vacuum chamber. The pyrometer is placed inside the chamber to avoid window corrections. A third laser directed at the sample from below through the nozzle is used to compensate the cooling of the sample by the gas flow. A high-quality video image of the sample taken from above is continuously displayed in order to monitor the levitation of the sample during heating. Video images of the sample are also displayed with a horizontal camera in order to determine the sample position in the levitator and to monitor the vertical stability.

2.3. Experimental configuration

A concise description of the D4c neutron diffractometer can be found in Fischer *et al* [18]. This is a two-axis instrument optimized for structural investigations of liquids and amorphous

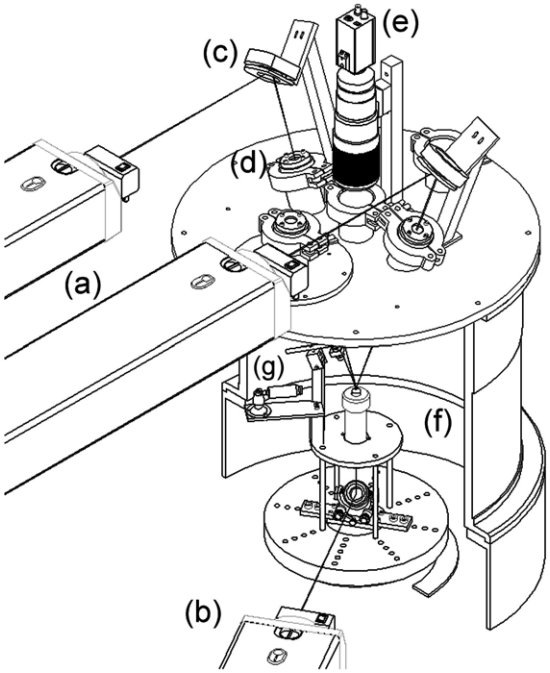

Figure 1. Schematic view of the experimental arrangement: laser heads ((a), (b)), spherical mirrors (c), NaCl windows (d), video camera (e), levitation device (f) and horizontal camera (g).

materials. It has basically three main components: the monochromator, the vacuum chamber and the detector. In this study, we used Cu[200] and Cu[220] monochromators giving working wavelengths of 0.7 and 0.5 Å. The actual values of wavelength and zero-angle shift are determined by means of a Rietveld refinement of a standard diffractogram (Ni powder). For both experiments we obtained 0.695 94 Å and 0.502 23 Å, and 0.023 9710° and −0.074 745°, respectively. The vacuum chamber consists of a cylinder 550 mm high and 460 mm in diameter in which the high-temperature device described above is enclosed. During experiments, the chamber is initially pumped down to low pressure (10^{-4} mbar) and then filled with the levitation gas up to atmospheric pressure. This ensures a reproducible atmosphere around the sample and is necessary for removing the background correctly during the data analysis. The entire vacuum chamber is cooled with circulating cooling water. The wide-angle detector is scanned over a 1.3–140° angular range giving scattering vector modulus Q ranges of 0.3–23 Å^{-1} at a wavelength of 0.5 Å and 0.2–16 Å^{-1} at 0.7 Å. The average resolution of the diffractometer is $\Delta Q/Q = 2.5 \times 10^{-2}$.

An assembly of vertical and horizontal isotopic $^{10}B_4C$ slits produced a rectangular beam on the sample. The beam size was around 5 mm vertically and 10 mm horizontally. The vertical slits were placed very near the nozzle and adjusted in order to mask the nozzle from the incident beam, thus avoiding any significant scattering from it. The actual irradiated sample volume needed for the data analysis was determined from the video image taken with the horizontal camera ((g) in figure 1).

2.4. Computational details

In order to understand our experimental data (which have not been resolved into partial structure factors) more clearly, and to reliably assign weak or 'noisy' features in $S(Q)$, we performed

Table 1. Characteristics of the samples simulated by AIMD.

			Number of atoms			
Sample	x	Side box (Å)	O	Al	Y	T (K)
AY15	0.15	13.17	90	51	9	2000
AY20	0.20	13.04	90	48	12	2150
AY25	0.25	12.93	90	45	15	2300
YAG	0.375	12.99	96	40	24	2300

AIMD simulations on the liquid Y_2O_3–Al_2O_3 systems. The calculations were performed with the Vienna *ab initio* simulation package (VASP) code [19–21], based on density functional theory (DFT) using a plane-wave basis set. Thereby we obtain the instantaneous electronic structure and the forces acting on atoms for every atomic configuration. The force acting on each atom is the essential quantity required to propagate the atomic coordinates in a time step of the MD simulation.

Our electronic calculations were performed at the Gamma point ($\boldsymbol{k} = 0$), using projector augmented wave (PAW) pseudopotentials [22] with the lowest plane wave cutoff and the Perdew–Burke–Ernzerhof (PBE) generalized gradient approximation functional. The atoms of the analysed samples (AY15, AY20, AY25 and YAG; see table 1 for details) were confined in a cubic box under periodic boundary conditions in a constant volume/temperature (NVT) ensemble. The time step was 2 fs for a total simulation time of 14 ps, except for the YAG which had a total simulation time of 20 ps. These DFT-based simulations are parameter-free and are performed independently of the experiments. While perfect agreement between simulation and experiment is unlikely in view of the lack of parameter-refinement, a reasonable agreement between the two approaches will allow the simulation models to be used to better understand the experimental data.

The AIMD trajectory was analysed using the nMoldyn program [23] in order to determine $S(Q)$ via the van Hove correlation functions. Other quantities such as $g_{ij}(r)$ were determined from a simple analysis of the time-dependent atomic coordinates.

3. Analysis of diffraction data

A recent description of the technique and theoretical background for x-ray and neutron diffraction studies with liquids and glasses can be found in Fischer *et al* [24]. In a neutron diffraction experiment from an n-component material the mean differential scattering cross section per atom can be written as

$$\frac{\mathrm{d}\sigma}{\mathrm{d}\Omega} = \sum_{i=1}^{n} c_i \bar{b}_i^2 + \left(\sum_{i=1}^{n} c_i \bar{b}_i \right)^2 (S(Q) - 1), \tag{1}$$

where c_i and b_i are, respectively, the atomic concentration and the coherent scattering length of species i present in the sample. All b_i values have been compiled by Sears [25]. The total pair correlation function $g(r)$ is calculated from the total structure factor $S(Q)$ using a classical Fourier transform:

$$g(r) = 1 + \frac{1}{2\pi^2 \rho_0} \int_0^{Q_{\max}} Q(S(Q) - 1) \frac{\sin Qr}{r} M(Q)\, \mathrm{d}Q \tag{2}$$

where ρ_0 is the number of atoms per unit volume. $M(Q)$ is a modification function $\sin(Q\pi/Q_{\max})/(Q\pi/Q_{\max})$ used to force the integrand to go smoothly to zero at $Q_{\max}$. The

Table 2. Neutron weighting factors W_{ij} for all studied compositions calculated using equation (4).

Sample	x	Al–O	Y–O	O–O	Y–Y	Y–Al	Al–Al
AY15	0.150	0.312	0.124	0.463	0.008	0.042	0.052
AY20	0.200	0.284	0.159	0.447	0.014	0.050	0.045
AY25	0.250	0.257	0.193	0.433	0.021	0.057	0.038
YAG	0.375	0.198	0.267	0.400	0.045	0.066	0.025

total structure factor and pair correlation functions are weighted sums of partial functions:

$$S(Q) = \sum_{i,j} W_{ij} S_{ij}(Q) \qquad \text{and} \qquad g(r) = \sum_{i,j} W_{ij} g_{ij}(r), \tag{3}$$

with

$$W_{ij} = \sum_{i,j} \frac{c_i c_j \bar{b}_i \bar{b}_j}{\left(\sum c_i \bar{b}_i\right)^2}. \tag{4}$$

The W_{ij} values have been calculated for all studied compositions and the results are given in table 2.

To extract the scattering cross section from the scattered intensity from the sample we first subtracted the scattering from the entire sample environment and from the absorption contribution and we normalized to a vanadium standard reference. This means that in addition to the measurement of the sample scattering, it is necessary to measure the diffracted intensity from the levitator alone, from a standard vanadium sample and from the empty diffractometer.

Since the nozzle was completely hidden by the bottom part of the slits, the relatively low background intensity was mostly due to scattering from the gas in the chamber.

4. Results

4.1. Experimental results

The neutron scattering measurements on the AY15 and AY25 sample were performed using a wavelength of 0.695 94 Å. With the YAG sample, the neutron data were obtained using a wavelength of 0.502 23 Å.

Figure 2 shows the total structure factors of liquid YAG, AY25 and AY15 at a temperature of 2373 K.

All curves are very similar and exhibit several peaks up to 16 $Å^{-1}$. For $x = 0.150$ (curve a), the main peak is found at 2.75 $Å^{-1}$. This position is shifted to higher Q when the yttria content is increased: 2.79 $Å^{-1}$ for $x = 0.250$ (b) and 2.84 $Å^{-1}$ for $x = 0.375$ (c1). According to the first MD simulations on yttrium aluminate glasses of Wilson and McMillan [6], this peak is dominated by the contribution of the O–O partial structure factor. From these simulations, the shift to larger Q can be explained by the increased contribution of the $S_{Y-O}(Q)$ partial structure factor.

A small peak on the left part of the main peak is found at 1.98 $Å^{-1}$ and is mainly due to $S_{Al-Y}(Q)$ and $S_{Y-Y}(Q)$ contributions [6]. For the YAG sample, we also reported the x-ray structure factor obtained at the same temperature (c2) [17]. In this case, weighing factors (at $Q = 0$) are respectively 0.193 and 0.158 for $S_{Al-Y}(Q)$ and $S_{Y-Y}(Q)$ and the first peak is much higher than with neutrons. As previously, this peak is shifted to higher Q and becomes a shoulder when the yttria content is increased. In this case, this is due to a stronger contribution of the Y–Y and Y–Al partial structure factors.

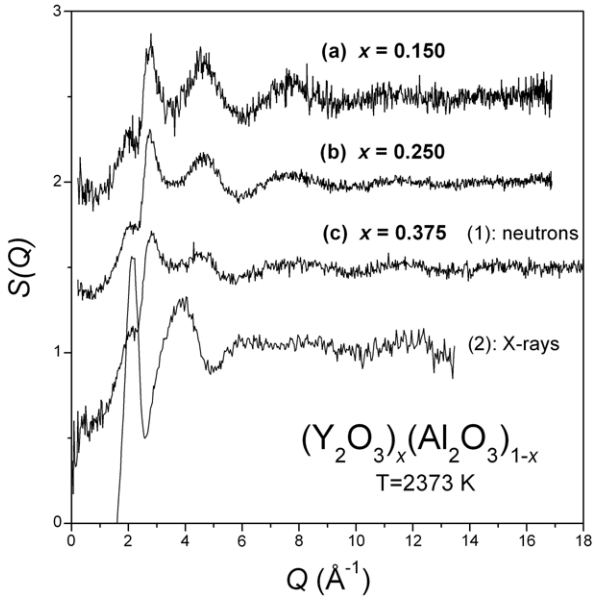

Figure 2. Total structure factors $S(Q)$ for liquid yttrium aluminates $(Y_2O_3)_x(Al_2O_3)_{1-x}$ at 2373 K for various yttria contents: $x = 0.150$ (a), $x = 0.250$ (b) and $x = 0.375$ (c). Curves are shifted up by 0.5 for clarity.

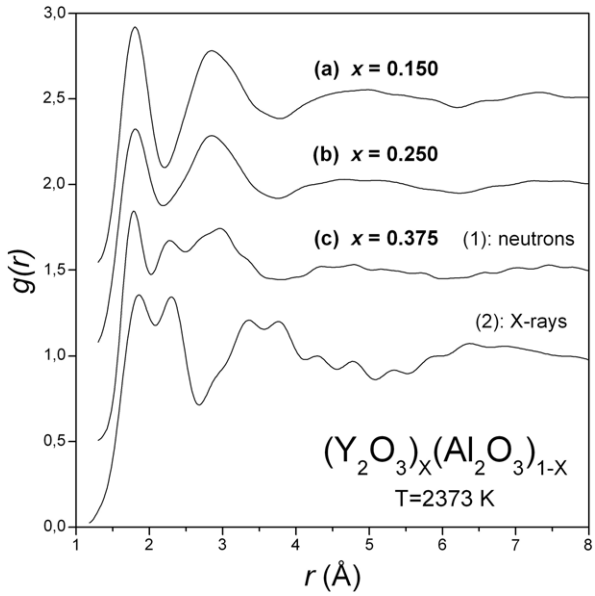

Figure 3. Total pair distribution functions $g(r)$ for liquid yttrium aluminates $(Y_2O_3)_x(Al_2O_3)_{1-x}$ at 2373 K for various yttria contents: $x = 0.150$ (a), $x = 0.250$ (b) and $x = 0.375$ (c). Curves are shifted up by 0.5 for clarity.

Figure 3 shows the corresponding total pair correlation $g(r)$ functions for the three compositions at 2373 K obtained by a Fourier transform of the previous $S(Q)$ using equation (2). Like $S(Q)$, $g(r)$ is dominated by the Al–O, Y–O and O–O partial functions

Table 3. Summary of the structural parameters determined experimentally.

	Q_1 (Å^{-1})	Q_2 (Å^{-1})	r Al–O	r Y–O	CN Al–O	CN Y–O
$X = 0.15$, AY15	1.98 ± 0.03	2.75 ± 0.05	1.81 ± 0.02	2.30 ± 0.1	4.3 ± 0.5	5.5 ± 0.5
$X = 0.25$, AY25	2.10 ± 0.03	2.79 ± 0.05	1.79 ± 0.02	2.30 ± 0.08	4.5 ± 0.5	5.6 ± 0.8
$X = 37.5$, YAG	2.15 ± 0.03	2.84 ± 0.05	1.78 ± 0.02	2.28 ± 0.04	4.4 ± 0.5	5.5 ± 1.0

for which the sum of the weighting factors is about 0.9 (see table 2). As previously, we also reported the x-ray pair correlation function obtained with liquid YAG (c2).

In order to determine the Al–O and Y–O coordination numbers (CN), we performed a Gaussian fit to the total correlation functions $T(r) = 4\pi r\rho_0 g(r)$, where ρ_0 is the atomic number density taken as 0.062, 0.067 and 0.074 atom Å^{-3} for AY15, AY25 and YAG, respectively.

In all curves, the first peak corresponds to the nearest-neighbour Al–O distance. Its position is found at 1.81 Å for AY15 (a), 1.79 Å for AY25 (b) and decreases down to 1.78 Å for the YAG composition (c1). These values are in good agreement with previous neutron works on glasses with the same compositions [5, 26] and x-ray studies on liquid YAG [13, 17]. The second peak is due to Y–O correlations and is found around 2.28 Å with the YAG sample. For AY25 the peak appears as a shoulder and is no longer visible with AY15. From the Gaussian fit, we estimated the Y–O distance to be 2.30 Å for these two compounds.

The interpretation of the following peaks is more difficult since all other correlations are involved, including O–O and cation–cation.

The area under the first peak gives an Al–O coordination number of around 4.4, in good agreement with previous NMR [12] and neutron scattering [5] measurements. These values are also consistent with the Al–O distances determined previously since typical Al–O distances are 1.75 Å and 1.90 Å for tetrahedral and octahedral sites, respectively. For liquid YAG, the second Gaussian gives a Y–O coordination number around 5.5. This value is obtained assuming a symmetrical Y–O peak and we will see later that it is underestimated. Similar coordination numbers have been found for the other compositions, but calculations were not easy since the Y–O peak is not easily visible. Consequently the obtained values have larger error bars. However, these values agree well with the previous x-ray work of Weber *et al* [13] on liquid YAG and are very close to the values determined by Wilding *et al* on the glasses using neutron scattering [5]. All the experimental results are summarized in table 3.

4.2. Simulation results

The partial pair distribution functions $g_{ij}(r)$ for liquid AY15, AY20, AY25 and YAG compounds calculated from AIMD simulations are shown in figures 4–7. In all figures the inset is a comparison of the calculated total structure factor $S(Q)$ and the experimental neutron diffraction data, except for the AY20 sample for which we have not been able to collect data.

All the $S(Q)$ show a very similar trend and the agreement between the simulated and experimental function is relatively good for the YAG composition (figure 7). Some discrepancies in the height of the peaks are visible for YA15 and YA25.

The pre-peak, which appears as a broad shoulder at 2.18 Å^{-1} is given by Al–Y and Y–Y correlations, as explained in the experimental part. The first main peak mostly due to O–O correlations is found at 2.8 Å^{-1} followed by a second one at higher Q at 4.6 Å^{-1}.

Figures 4–7 also show all the calculated partial pair distribution functions $g_{ij}(r)$. Although there are some discrepancies, in particular around the Y–O contribution, we found in all cases

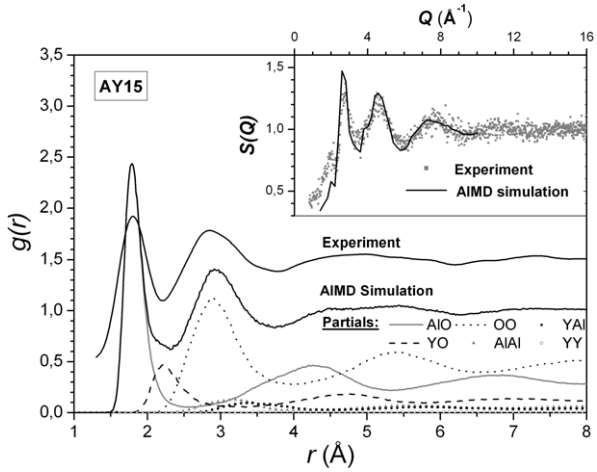

Figure 4. Total pair distribution function $g(r)$ for liquid AY15 at 2373 K: comparison between experiment and AIMD simulations (the experimental curve is shifted up). The lower curves depict the six partial pair distribution functions obtained from the simulations. The inset shows the experimental total structure factor $S(Q)$ as compared to the simulation results.

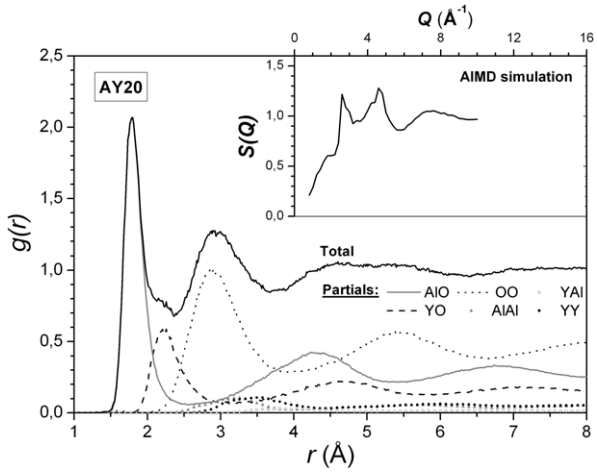

Figure 5. Calculated total pair distribution function $g(r)$ for liquid AY20 at 2373 K. The lower curves depict the six partial pair distribution functions obtained from the simulations. The inset shows the calculated total structure factor $S(Q)$.

a reasonably good agreement between the experimental and calculated $g(r)$. These partial pair correlation functions enable us to determine precisely the contribution of all correlations to each peak which is helpful for the data interpretation. All calculated parameters (distances and coordination numbers) are summarized in table 4.

From the AIMD simulations we found an Al–O bond distance of 1.81 Å, identical for all samples. As observed previously with liquid YAG [17], the Y–O partial correlation function $T_{\mathrm{Y-O}}(r)$ exhibits a shoulder on its high-r side for all compositions. This can be explained by the existence of two Y–O distances in the liquid state as observed in the crystalline phases. Figure 8 shows the Y–O partial correlation function for AY15 and the fit of the first peak using two Gaussians. We found two Y–O bond distances around 2.2 and 2.5 Å. This observation is

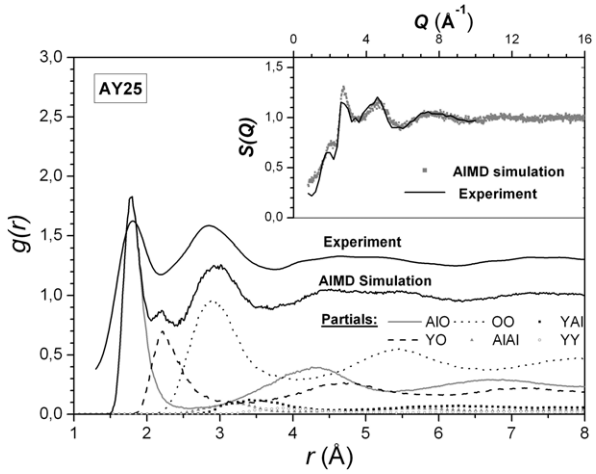

Figure 6. Total pair distribution function $g(r)$ for liquid AY25 at 2373 K: comparison between experiment and AIMD simulations (the experimental curve is shifted up). The lower curves depict the six partial pair distribution functions obtained from the simulations. The inset shows the experimental total structure factor $S(Q)$ as compared to the simulation results.

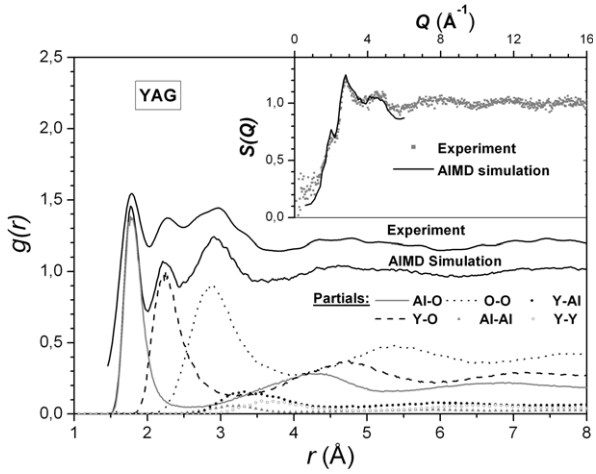

Figure 7. Total pair distribution function $g(r)$ for liquid YAG at 2373 K: comparison between experiment and AIMD simulations (the experimental curve is shifted up). The lower curves depict the six partial pair correlation functions obtained from the simulations. The inset shows the experimental total structure factor $S(Q)$ as compared to the simulation results.

not possible using the experimental total pair distribution function $g(r)$ where we can see only one peak at 2.34 Å. This shows that the data interpretation is not easy without information on the partial $g(r)$. The distances obtained with the other samples do not change significantly and are summarized in table 4.

The third peak in $g(r)$ is mainly due to the contribution of O–O correlations and the partial correlation function $T_{O-O}(r)$ presented in figure 8 for the case of YA15 can be also modelled using a double peak. The first one is located around 2.8 Å. This value is very close to the O–O bond distance found in liquid Al_2O_3 [27] and could correspond to the distance between oxygen

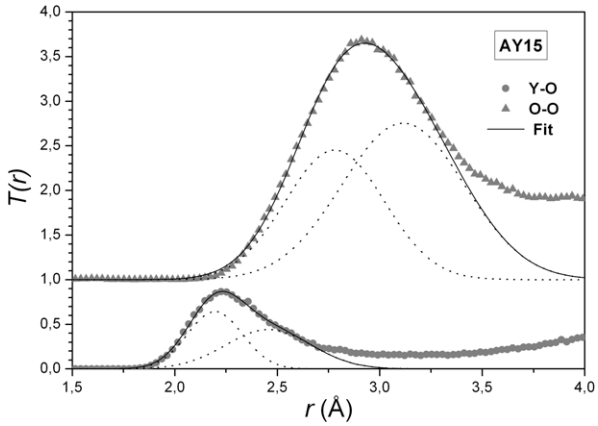

Figure 8. Y–O and O–O correlation functions from AIMD simulations. Both curves are fitted with two Gaussians leading to two distances for Y–O and O–O bonds.

Table 4. Nearest-neighbour interatomic distances and coordination numbers for AY15, AY20, AY25 and YAG from AIMD simulations.

Sample	r AlO (Å)	r YO (Å)	r OO (Å)	CN AlO	CN YO
YA15	$r_1 = 1.81$	$r_1 = 2.20$ $r_2 = 2.46$	$r_1 = 2.8$ $r_2 = 3.1$	4.2 ± 0.3	6.1 ± 1.1
YA20	$r_1 = 1.81$	$r_1 = 2.20$ $r_2 = 2.50$	$r_1 = 2.8$ $r_2 = 3.2$	4.2 ± 0.3	6.1 ± 1.0
YA25	$r_1 = 1.81$	$r_1 = 2.21$ $r_2 = 2.51$	$r_1 = 2.8$ $r_2 = 3.2$	4.2 ± 0.3	6.4 ± 1.0
YAG	$r_1 = 1.81$	$r_1 = 2.22$ $r_2 = 2.53$	$r_1 = 2.8$ $r_2 = 3.2$	4.3 ± 0.4	6.8 ± 1.1

atoms around Al. If Al is tetrahedrally coordinated, then the shortest O–O distance is equal to $r_{\mathrm{Al-O}} \times 1.633 = 2.9$ Å, very close to the determined peak position.

The second peak is found at about 3.2 Å, very close to the O–O bond length of 3.06 Å found in liquid Y_2O_3 [28]. In this case it could correspond to the distance between oxygen atoms around Y. If Y is octahedrally coordinated as seen experimentally, then the calculated shortest O–O distance is $r_{\mathrm{Y-O}} \times \sqrt{2} = 3.3$ Å. Similar calculations can be performed for all other samples and the results are summarized in table 4.

The determination of the coordination numbers is performed by counting the number of atoms within the cutoff radius of 2.5 Å for Al–O and 3.3 Å for Y–O.

For Al–O bonds, the average coordination is found around 4.2 for all compositions, in agreement with experimental values.

For Y–O bonds, we notice a slight increase of the coordination with the increase of the Y_2O_3 content with values from 6.1 (YA15) to 6.8 (YAG). In particular, the latest one is close to the value 7.3 found for liquid YAG using x-ray absorption spectroscopy [15].

5. Conclusion

We have combined aerodynamic levitation and laser heating with neutron diffraction to study the structure of liquid yttrium aluminates. We found experimentally that Al and Y atoms are, respectively, tetrahedrally and octahedrally coordinated for all the studied compositions.

From *ab initio* molecular dynamics simulations, we found Y–O coordination numbers of slightly more than 6 for low yttria contents and a value close to 7 for the YAG composition as observed in other study [14]. This shows that Y–O coordination numbers calculated directly from a Gaussian fit to $T(r)$ are underestimated. This is mostly due to the influence of O–O and cation–cation correlations which are close to the Y–O peak in the experimental $g(r)$ and make the interpretation relatively difficult.

This study shows that the use of simulation techniques is important for deriving reliable structural information from liquid materials.

These AIMD simulations are in relatively good agreement with the experimental diffraction data. Further calculations are in progress to determine the bond angle distributions.

Acknowledgments

The authors are particularly grateful to P Palleau and to the staff of the Computing Group at the ILL for their technical assistance, to S Brassamin and Ph Melin for the design and development of the experimental setup and to C A Angell for helpful discussions. The financial support of the ILL's Diffraction Group in making the set-up is also particularly acknowledged. Q Vu Van would like to thank the Science and Technology Facility Council for financial support. G N Greaves and M C Wilding acknowledge support from the Higher Education Funding Council for Wales through the Centre for Advanced Functional Materials and Devices.

References

[1] Wilding M C and McMillan P F 2001 *J. Non-Cryst. Solids* **293–295** 357–65
[2] Wilding M C, McMillan P F and Navrotsky A 2002 *Physica* A **314** 379–90
[3] Greaves G N and Sen S 2007 *Adv. Phys.* **56** 1–166
[4] McMillan P F, Wilson M and Wilding M C 2003 *J. Phys.: Condens. Matter* **15** 6105–21
[5] Wilding M C, Benmore C J and McMillan P F 2002 *J. Non-Cryst. Solids* **297** 143–55
[6] Wilson M and McMillan P F 2004 *Phys. Rev.* B **69** 054206
[7] Yu D L and Tang D Y 2003 *Opt. Laser Technol.* **35** 37–42
[8] Bressi G, Carugno G, Conti E, Del Noce C and Iannuzzi D 2001 *Nucl. Instrum. Methods Phys. Res.* A **461** 361–4
[9] Gervais M, Le Floch S, Rifflet J-C, Coutures J and Coutures J-P 1992 *J. Am. Ceram. Soc.* **75** 3166–8
[10] Coutures J, Rifflet J-C, Billard D and Coutures J-P 1987 *Eur. Space Agency Spec. Rep.* **256** 427–30
[11] Medraj M, Hammond R, Parvez M A, Drew R A L and Thompson W T 2006 *J. Eur. Ceram. Soc.* **26** 3515–24
[12] Coutures J-P, Massiot D, Bessada C, Echegut P, Rifflet J-C and Taulelle F 1990 *C. R. Acad. Sci.* **310** 1041–5
[13] Weber J K R, Krishnan S, Ansell S, Hixson A D and Nordine P C 2000 *Phys. Rev. Lett.* **84** 3622–5
[14] Cristiglio V *et al* 2007 *J. Non-Cryst. Solids* **353** 1789–92
[15] Landron C, Hennet L, Coutures J-P, Gailhanou M, Gramond M and Bérar J-F 1998 *Europhys. Lett.* **44** 429–35
[16] Wilding M C, Greaves N G, Benmore C J and Weber J K R 2006 *Proc. SRMS-5 Conf. (Chicago)* pp 299–300
[17] Hennet L *et al* 2006 *Rev. Sci. Instrum.* **77** 053903
[18] Fischer H E, Cuello G J, Palleau P, Feltin D, Barnes A C, Badyal Y S and Simonson J M 2002 *Appl. Phys.* A **74** 160–2
[19] Kresse G and Hafner J 1993 *Phys. Rev.* B **47** 558–61
[20] Kresse G and Furthmuller J 1996 *Phys. Rev.* B **54** 11169–86
[21] Kresse G and Furthmuller J 1996 *Comput. Mater. Sci.* **6** 15–50
[22] Kresse G and Joubert D 1999 *Phys. Rev.* B **59** 1758–75
[23] Róg T, Murzyn K, Hinsen K and Kneller G R 2003 *J. Comput. Chem.* **24** 657–67
[24] Fischer H E, Barnes A C and Salmon P S 2006 *Rep. Prog. Phys.* **69** 233–99
[25] Sears V F 1992 *Neutron News* **3** 26–37
[26] Rix J E, Weber J K R, Santodonato L J, Hammons S E, Hodges J, Rennich M and Volin K J 2006 *Proc. ICANS-XVII (Santa Fe)* vol III pp 1086–95
[27] Krishnan S and Price D L 2000 *J. Phys.: Condens. Matter* **12** R145–76
[28] Hennet L, Thiaudière D, Landron C, Melin P, Price D L, Bérar J-F and Saboungi M-L 2003 *Appl. Phys. Lett.* **83** 3305–7